

Coupled Henon Map, Part I: Topological Horseshoes and Uniform Hyperbolicity

Keisuke Fujioka¹, Ryota Kogawa¹, Jizhou Li² and Akira Shudo¹

¹ Department of Physics, Tokyo Metropolitan University, Tokyo 192-0397, Japan

² RIKEN iTHEMS, Wako, Saitama 351-0198, Japan

Abstract. We derive a sufficient condition for topological horseshoe and uniform hyperbolicity of a 4-dimensional symplectic map, which is introduced by coupling the two 2-dimensional Hénon maps via linear terms. The coupled Hénon map thus constructed can be viewed as a simple map modeling the horseshoe in higher dimensions. We show that there are two different types of horseshoes, each of which is realized around different anti-integrable limits in the parameter regime.

1. Introduction

Horseshoe dynamics is known to be a source of chaos in dynamical systems. The most well-known and the simplest system modeling the horseshoe dynamics would be the Hénon map [1, 2], which is a 2-dimensional quadratic map defined on \mathbb{R}^2 . In the 2-dimensional plane, the horseshoe-shaped deformation is obtained by first stretching some initial domain in the unstable direction and then contracting it in the stable direction after folding back the stretched domain.

Suppose that the horseshoe-shaped domain, in both forward and backward iterations, intersects the original domain with two distinct regions, each of which is completely penetrated without lateral overhang. In this case, we say that the dynamics exhibits *topological horseshoe* [3, 4]. When the topological horseshoe is realized, the intersection of the iterated domain with the original domain, which generates the two disjoint strips in the case of a once-fold dynamics, is always mapped into the previous intersections, meaning that the width of each strip gradually decreases in time. Furthermore, if the contraction in the domain of interest is exponentially fast, each strip will eventually shrink to a string. If this is also the case in the backward iteration, the strings formed in the stretching and contracting directions iterates intersect to give a set of points. It then leads to the conjugation relation between the original and the properly introduced symbolic dynamics. The so-called Conley-Moser theory concerns a sufficient condition to have the symbolic dynamics based on topological horseshoe and *uniform hyperbolicity* [5].

For the Hénon map, Devaney-Nitecki first developed such an argument and gave a sufficient condition such that the Hénon map exhibits topological horseshoe and uniform hyperbolicity as well [6]. Later, it was proved that the parameter locus satisfying uniform hyperbolicity can be extended to the situation where the first homoclinic tangency happens using the complex dynamics technique [7] and computer-assisted proof [8, 9].

There is another, even simpler approach to capturing the existence of chaos. Suppose that the system has a certain parameter whose limiting value kills the dynamical relation between successive time steps, resulting in an infinite sequence of numbers or symbols. Such a limit is called the *anti-integrable limit* [10–12]. Suppose there exists a suitable (discrete) Lagrangian. Then one can find a one-to-one correspondence between a sequence of numbers in the anti-integrable limit and an orbit generated by the actual dynamics whose parameter is close to the anti-integrable limit. The proof is based on the global implicit function theorem and the contraction mapping principle can be easily generalized to a wide class of systems. Moreover, since a close analogy exists between the orbits in dynamical systems and the equilibrium states of a class of variational problems in solid-state systems, one can relate the uniform hyperbolicity of the dynamics with the existence of phonon gap in the solid state problem [13].

The topic we would like to discuss in this article is the topological horseshoe and uniform hyperbolicity in higher dimensional symplectic maps. Among a variety of choices [14–30], we here take the coupled Hénon map, which will be introduced below. As

in the case of 2-dimensional polynomial maps [31], there is a derivation of normal forms of quadratic symplectic maps due to Moser [32], which provides a canonical model to be studied in detail [29,30]. Indeed, it was shown in [30] that the normal form introduced by Moser can be decoupled into a pair of uncoupled quadratic maps under an appropriate choice of parameters, so our map should be a reduced version of the general normal form.

An advantage of starting with the coupled Hénon map to examine topological horseshoes and uniform hyperbolicity would be that one can find anti-integrable limits in the parameter space rather easily. As mentioned above, one would expect uniform hyperbolicity, and perhaps also topological horseshoe as well in the vicinity of anti-integrable limits [34, 38–41]. There indeed exist some works in which topological horseshoe together with uniform hyperbolicity manifests in the region close to the anti-integrable limit [36, 37].

Here we provide a sufficient condition for topological horseshoe and uniform hyperbolicity for the coupled Hénon map, using essentially the same strategy as Devaney-Nitecki [6]. In particular, we study topological horseshoe and uniform hyperbolicity around the two different anti-integrable limit, each of which is derived by taking certain parameter limits in the coupled Hénon map. The first type can be shown to be conjugate with the symbolic dynamics with four symbols, while the second one is described by the full shift with two symbols. As will be briefly explained and thoroughly discussed in the following paper, their folding natures are different from each other. Especially the first type is so unique that it appears only in 4-dimensional space.

The structure of the paper is as follows: Section 2 introduces our coupled Hénon map, which is obtained by coupling a pair of 2-dimensional Hénon maps, and has three parameters: the two nonlinearity parameters and the coupling strength. Then we show that two anti-integrable limits exist in the current form of the coupled Hénon map. Section 3 gives the main results of this paper, providing a sufficient condition for topological horseshoe and uniform hyperbolicity around each anti-integrable limit. Section 4 presents the existence domains in which the non-wandering set is contained. This part corresponds to the proof of the first part of the main theorems. Section 5 gives a sufficient condition for uniform hyperbolicity of the coupled Hénon map. To derive uniform hyperbolicity, we examine the cone field condition. In particular, we will use a sufficient condition for uniform hyperbolicity in higher dimensional settings, which have been introduced by Newhouse [42]. Section 6 is devoted to proving the main theorems. Section 7 summarizes the results and provides some outlooks.

2. Coupled Hénon map and anti-integrable limits

2.1. Coupled Hénon map

The coupled Hénon map is introduced as

$$\begin{pmatrix} x_{n+1} \\ y_{n+1} \\ z_{n+1} \\ w_{n+1} \end{pmatrix} = f \begin{pmatrix} x_n \\ y_n \\ z_n \\ w_n \end{pmatrix} = \begin{pmatrix} a_0 - x_n^2 - z_n + c(x_n - y_n) \\ a_1 - y_n^2 - w_n - c(x_n - y_n) \\ x_n \\ y_n \end{pmatrix}, \quad (2.1)$$

where $c > 0$ is assumed. The inverse map f^{-1} is

$$\begin{pmatrix} x_{n-1} \\ y_{n-1} \\ z_{n-1} \\ w_{n-1} \end{pmatrix} = f^{-1} \begin{pmatrix} x_n \\ y_n \\ z_n \\ w_n \end{pmatrix} = \begin{pmatrix} z_n \\ w_n \\ a_0 - z_n^2 - x_n + c(z_n - w_n) \\ a_1 - w_n^2 - y_n - c(z_n - w_n) \end{pmatrix}. \quad (2.2)$$

Here a_0 and a_1 are parameters that control the nonlinearity, and the parameter c gives the coupling strength between the two Hénon maps [6]. For $c > 0$, the replacement of the variables as $(x, y, z, w) \rightarrow (z, w, x, y)$ transforms the map f into its inverse f^{-1} .

$$\begin{pmatrix} X \\ Y \\ Z \\ W \end{pmatrix} = \frac{1}{2} \begin{pmatrix} x + y \\ x - y \\ z + w \\ z - w \end{pmatrix}, \quad (2.3)$$

the form (2.1) can be written as

$$\begin{pmatrix} X_{n+1} \\ Y_{n+1} \\ Z_{n+1} \\ W_{n+1} \end{pmatrix} = F \begin{pmatrix} X_n \\ Y_n \\ Z_n \\ W_n \end{pmatrix} = \begin{pmatrix} A_0 - (X_n^2 + Y_n^2) - Z_n \\ A_1 - 2X_n Y_n - W_n + 2cY_n \\ X_n \\ Y_n \end{pmatrix}. \quad (2.4)$$

where

$$A_0 = \frac{a_0 + a_1}{2}, \quad A_1 = \frac{a_0 - a_1}{2}.$$

The inverse map F^{-1} is also rewritten as

$$\begin{pmatrix} X_{n-1} \\ Y_{n-1} \\ Z_{n-1} \\ W_{n-1} \end{pmatrix} = F^{-1} \begin{pmatrix} X_n \\ Y_n \\ Z_n \\ W_n \end{pmatrix} = \begin{pmatrix} Z_n \\ W_n \\ A_0 - (Z_n^2 + W_n^2) - X_n \\ A_1 - 2Z_n W_n - Y_n + 2cW_n \end{pmatrix}. \quad (2.5)$$

2.2. Anti-integrable limits for the coupled Hénon map

Here we show that two types anti-integrable limits exist in the coupled Hénon map. For simplicity, we consider the case with $a = a_0 = a_1$. Let us introduce new parameters $\epsilon = \sqrt{1/a}$, $u = \epsilon x$ and $v = \epsilon y$ and rewrite the coupled Hénon map (2.1) as

$$\begin{cases} \epsilon u_{n+1} = 1 - (u_n)^2 - \epsilon u_{n-1} + c\epsilon(u_n - v_n), \\ \epsilon v_{n+1} = 1 - (v_n)^2 - \epsilon v_{n-1} - c\epsilon(u_n - v_n). \end{cases} \quad (2.6)$$

(A) Anti-integrable limit with four symbols

The first type of anti-integrable limit is given by letting $a \rightarrow \infty$ with c being fixed. In this anti-integrable limit, the coupling between two Hénon maps can be neglected and (2.6) tends to

$$\begin{cases} 0 = 1 - (u_n)^2, \\ 0 = 1 - (v_n)^2, \end{cases} \quad (2.7)$$

which lead to

$$\begin{cases} u_n = \pm 1, \\ v_n = \pm 1. \end{cases} \quad (2.8)$$

The four solutions $(u_n, v_n) = (+1, +1), (+1, -1), (-1, +1), (-1, -1)$ provide symbols of the symbolic dynamics around this anti-integrable limit.

(B) Anti-integrable limit with two symbols

The second type of anti-integrable limit is given by letting $a \rightarrow \infty$ with $c/\sqrt{a} = \text{const} = \gamma$ being fixed. In this limit, the two Hénon maps are strongly coupled and the relations (2.6) tend to

$$\begin{cases} 0 = 1 - (u_n)^2 + \gamma(u_n - v_n), \\ 0 = 1 - (v_n)^2 - \gamma(u_n - v_n), \end{cases} \quad (2.9)$$

which lead to the four solutions in the form $(u_n, v_n) = (+1, +1), (\gamma - \sqrt{1 - \gamma^2}, \gamma + \sqrt{1 - \gamma^2}), (\gamma + \sqrt{1 - \gamma^2}, \gamma - \sqrt{1 - \gamma^2})$ and $(-1, -1)$. For $1 \leq |\gamma|$, the two solutions are complex, while for $1 > |\gamma|$ all the solutions are real.

3. Main theorems

In this paper, we will give sufficient conditions for topological horseshoe and uniform hyperbolicity around the anti-integrable limits (A) and (B), respectively.

Theorem 3.1. *As for the anti-integrable limit of the case (A), the following holds.*

A-1) For $-1 \leq A_0$, the non-wandering set $\Omega(f)$ satisfies

$$\Omega(f) \subset V_f, \quad (3.10)$$

where

$$V_f = \{(x, y, z, w) \mid |x|, |y|, |z|, |w| \leq r\}. \quad (3.11)$$

Here, $r = 2\sqrt{2}(1 + \sqrt{1 + A_0})$.

A-2) If the parameters satisfy the following conditions, f shows topological horseshoe.

$$0 < \frac{1}{4}c^2 + a_i - (c + 2)r, \quad (i = 0, 1), \quad (3.12)$$

$$0 \leq r^2 - 2(c + 1)r - a_i, \quad (i = 0, 1). \quad (3.13)$$

A-3) In addition to the conditions (3.12) and (3.13), if the parameters satisfy the following condition, $\Omega(f)$ is uniformly hyperbolic.

$$4 + c < \frac{-c + \sqrt{c^2 + 4(a_i - (c + 2)r)}}{2}, \quad (i = 0, 1). \quad (3.14)$$

Theorem 3.2. As for the anti-integrable limit of the case (B), the following holds.

B-1) For $-1 \leq A_0$, the non-wandering set $\Omega(f)$ satisfies

$$\Omega(f) \subset V_F, \quad (3.15)$$

where

$$V_F = \{(x, y, z, w) \mid \left| \frac{x+y}{2} \right|, \left| \frac{x-y}{2} \right|, \left| \frac{z+w}{2} \right|, \left| \frac{z-w}{2} \right| \leq R\}, \quad (3.16)$$

where $R = 1 + \sqrt{1 + A_0}$.

B-2) If the parameters satisfy the following conditions, f shows topological horseshoe.

$$A_1 \leq R < c, \quad (3.17)$$

$$R < A_0 - (W^*)^2 - R, \quad (3.18)$$

$$W^* \leq R. \quad (3.19)$$

Here, $W^* = \max\left(\left| \frac{2R - A_1}{2(c - R)} \right|, \left| \frac{-2R - A_1}{2(c - R)} \right| \right)$, and $Z^* = \sqrt{A_0 - (W^*)^2 - 2R}$.

B-3) In addition to the conditions (3.17), (3.18) and (3.19), if the parameters satisfy the following condition, $\Omega(f)$ is uniformly hyperbolic.

$$4 + c \leq Z^* - W^*. \quad (3.20)$$

4. Non-wandering set

4.1. Some lemmas

To prove topological horseshoe and uniformly hyperbolicity for the coupled Hénon map we take a similar strategy similar to Devaney-Nitecki [6]. In the following, we prove some lemmas using the parameter:

$$R = 1 + \sqrt{1 + A_0} \in \mathbb{R}. \quad (4.1)$$

Lemma 4.1. R satisfies the following

$$R^2 - 2R - A_0 = 0. \quad (4.2)$$

Proof. Self-evident. □

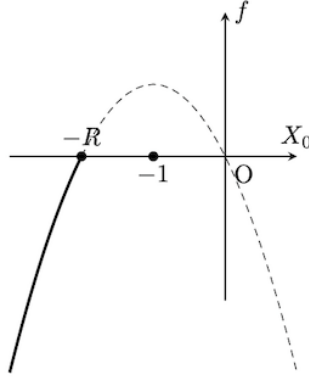


Figure 1: Sketch of $f = A_0 - (X_0)^2 - 2X_0$.

Lemma 4.2. a) For any $C \geq 0$, if $|Z_0| \leq C$ is satisfied, the following holds:

$$A_0 - (Z_1^2 + W_1^2) - C \leq X_1 \leq A_0 - (Z_1^2 + W_1^2) + C. \quad (4.3)$$

In addition, if $|X_0| \leq C$, then $|Z_1| \leq C$ holds.

b) For any $C \geq 0$, if $|X_0| \leq C$ is satisfied, the following holds:

$$A_0 - (X_{-1}^2 + Y_{-1}^2) - C \leq Z_{-1} \leq A_0 - (X_{-1}^2 + Y_{-1}^2) + C. \quad (4.4)$$

In addition, if $|Z_0| \leq C$, then $|X_{-1}| \leq C$ holds.

Proof. It is easy to check both of them. □

Lemma 4.3. a) If $X_0 \leq \min(-|Z_0|, -R)$, then $X_1 \leq X_0$ follows. The equality holds when $(X_0, Y_0, Z_0) = (-R, 0, -R)$.

b) If $-|Z_0| \leq X_0$ and $Z_0 \leq -R$ hold, then $Z_{-1} \leq Z_0$ and $|Z_0| \leq |Z_{-1}|$ follows. The equalities hold when $(X_0, Z_0, W_0) = (-R, -R, 0)$.

Proof. a) If $X_0 \leq \min(-|Z_0|, -R)$ holds, we find that

$$\begin{aligned} X_1 - X_0 &= A_0 - (X_0^2 + Y_0^2) - Z_0 - X_0 \\ &\leq A_0 - X_0^2 - Z_0 - X_0 \\ &\leq A_0 - X_0^2 + |Z_0| - X_0 \\ &\leq A_0 - X_0^2 - 2X_0 \\ &= A_0 - (X_0 + 1)^2 + 1. \end{aligned} \quad (4.5)$$

Since $X_0 \leq -R$, we have a condition for X_0 as

$$X_0 \leq -R = -1 - \sqrt{1 + A_0} \leq -1. \quad (4.6)$$

Then, $A_0 - (X_0 + 1)^2 + 1$ takes the maximum value at $X_0 = -R$ (see Fig. 1). Thus, we have

$$X_1 - X_0 \leq A_0 - (-R)^2 - 2(-R) = 0. \quad (4.7)$$

Here we have used lemma 4.1. The equality holds when $(X_0, Y_0, Z_0) = (-R, 0, -R)$ is satisfied.

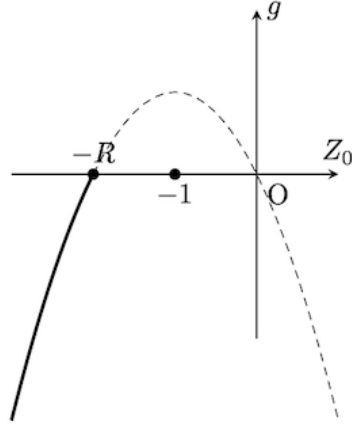


Figure 2: Sketch of $g = A_0 - (Z_0)^2 - 2Z_0$.

b) Assuming $-|Z_0| \leq X_0$ and $Z_0 \leq -R$, we find that

$$\begin{aligned}
 Z_{-1} - Z_0 &= A_0 - (Z_0^2 + W_0^2) - X_0 - Z_0 \\
 &\leq A_0 - Z_0^2 - X_0 - Z_0 \\
 &\leq A_0 - Z_0^2 + |Z_0| - Z_0 \\
 &= A_0 - Z_0^2 - 2Z_0 \\
 &= A_0 - (Z_0 + 1)^2 + 1.
 \end{aligned} \tag{4.8}$$

In the same way as above, since

$$Z_0 \leq -R \leq -1 \tag{4.9}$$

holds, $A_0 - (Z_0 + 1)^2 + 1$ takes the maximum value at $Z_0 = -R$ (see Fig. 2). Hence, we have

$$Z_{-1} - Z_0 \leq A_0 - (-R)^2 - 2(-R) = 0. \tag{4.10}$$

Since $Z_0 \leq -R$, $|Z_{-1}| \geq |Z_0|$ also follows. The equality holds when $(X_0, Z_0, W_0) = (-R, -R, 0)$ holds. \square

4.2. Decomposition of domains and transition rules

In the following, we study the coupled Hénon map in the case where R takes a real value. For this purpose, we introduce the following domains (see Fig. 3):

$$N_1 = \{(X, Y, Z, W) \mid X \leq \min(-|Z|, -R)\}, \tag{4.11}$$

$$N_2 = \{(X, Y, Z, W) \mid X \geq -R, |Z| \leq R\}, \tag{4.12}$$

$$N_3 = \{(X, Y, Z, W) \mid X \geq -|Z|, Z \geq R\}, \tag{4.13}$$

$$N_4 = \{(X, Y, Z, W) \mid X \geq -|Z|, Z \leq -R\}, \tag{4.14}$$

$$\tag{4.15}$$

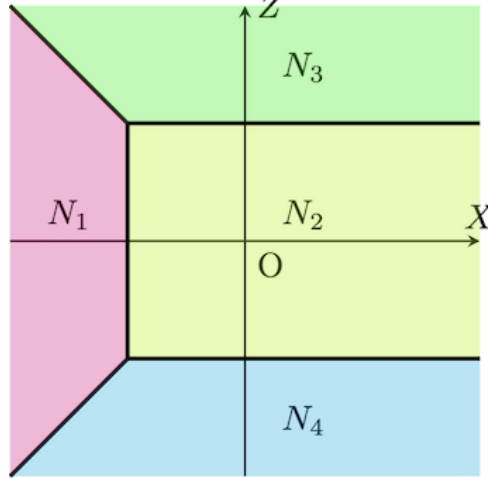


Figure 3: Illustration of domains and their boundary lines in the (X, Z) -plane.

Proposition 4.4. *If $A_0 \geq -1$, the following holds:*

- a) *Under the iteration of F , the coordinate X strictly decreases in N_1 except for $(X, Z) = (-R, -R)$.*
- b) *$F(N_1) \subset N_1$.*
- c) *$F(N_2) \subset N_1 \cup N_2$ and $F(N_3) \subset N_1 \cup N_2$.*
- d) *Under the iteration of F^{-1} , the coordinate Z strictly decreases in N_4 except for $(X, Z) = (-R, -R)$.*
- e) *$F^{-1}(N_3) \subset N_4$ and $F^{-1}(N_4) \subset N_4$.*
- f) *$F^{-1}(N_2) \subset N_2 \cup N_3 \cup N_4$.*

Proof. a) Self-evident from lemma 4.3 a).

b) For $(X_0, Y_0, Z_0, W_0) \in N_1$, $X_1 \leq X_0$ follows from a). From Eq. (2.4), we have $Z_1 = X_0 \leq -R < 0$. So, we have $-|Z_1| = X_0$, which leads to the inequality $X_1 \leq -|Z_1|$. In addition, $X_1 \leq X_0 \leq -R$ follows from a). Combining these, $(X_1, Y_1, Z_1, W_1) \in N_1$ is satisfied, *i.e.*, $F(N_1) \subset N_1$ holds.

c) Using lemma 4.2 by setting $C = R$, the region specified by $|Z| \leq R$, which covers the domain N_2 , is mapped to the horseshoe-shaped domain (see Fig. 4):

$$A_0 - (Z_1^2 + W_1^2) - R \leq X_1 \leq A_0 - (Z_1^2 + W_1^2) + R. \quad (4.16)$$

The right boundary is expressed as

$$X_1 = A_0 - (Z_1^2 + W_1^2) + R. \quad (4.17)$$

Since W_1 is real, X_1 is bounded as

$$X_1 \leq A_0 - Z_1^2 + R. \quad (4.18)$$

The boundary of Eq. (4.18), namely,

$$X_1 = A_0 - Z_1^2 + R, \quad (4.19)$$

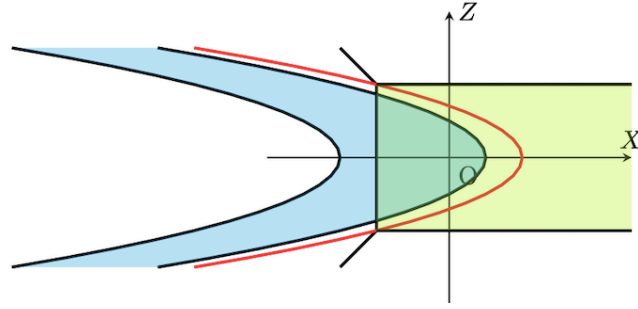


Figure 4: The blue region shows the horseshoe region obtained by setting $C = R$ in (4.3). The red curve is the parabola in Eq. (4.19).

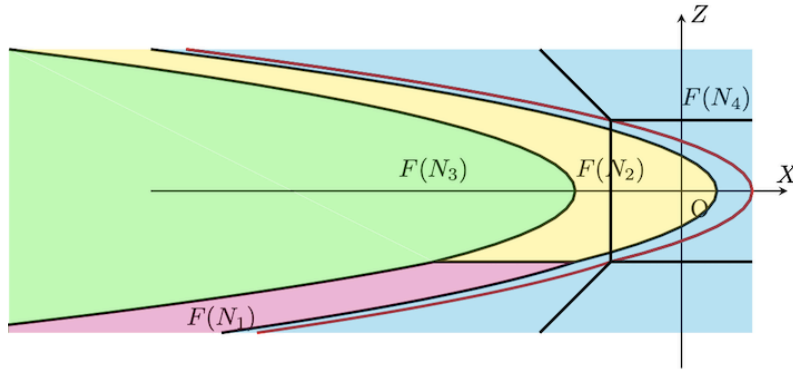


Figure 5: The iterated domains. The red curve represents the rightmost curves for the regions $F(N_1)$, $F(N_2)$ and $F(N_3)$.

is shown by the red curve in Fig. 4. Using lemma 4.1, it is easy to check that the point $(X_1, Z_1) = (-R, \pm R)$ satisfies Eq. (4.19). Therefore, the horseshoe-shaped region, specified by Eq. (4.16), lies completely inside the left-hand side of the red curve expressed by Eq. (4.19), and the red curve passes through the corner points $(X_1, Z_1) = (-R, \pm R)$ of N_2 . Thus, $F(N_2) \subset N_1 \cup N_2$ is concluded. It is also easy to show that the line $Z = R$ is mapped to the leftmost curve shown in Fig. 4. As a result, $F(N_3) \subset N_1 \cup N_2$ follows (see Fig. 5). d) Self-evident from lemma 4.3 b).

e) Note that the domain N_3 in (X, Z) -plane is expressed as

$$N_3 = \{(X, Y, Z, W) \mid Z = -X + \gamma, \gamma \geq 0, Z \geq R\}, \quad (4.20)$$

thus it is mapped by F^{-1} as

$$F^{-1}(N_3) = \{(X, Y, Z, W) \mid Z = A_0 - (X^2 + Y^2) + X - \gamma, \gamma \geq 0, X \geq R\}. \quad (4.21)$$

For $\gamma \geq 0$, we find that $Z = A_0 - (X^2 + Y^2) + X - \gamma \leq A_0 - X^2 + X \leq -R$. Here we have used lemma 4.1 and $X \geq R$ in the region $F^{-1}(N_3)$. Since the points in $F^{-1}(N_3)$ satisfy $X \geq R$ and $Z \leq -R$, $F^{-1}(N_3) \subset N_4$ holds.

In a similar way, the domain N_4 is expressed as

$$N_4 = \{(X, Y, Z, W) \mid Z = X - \gamma, Z \leq -R, \gamma \geq 0\}, \quad (4.22)$$

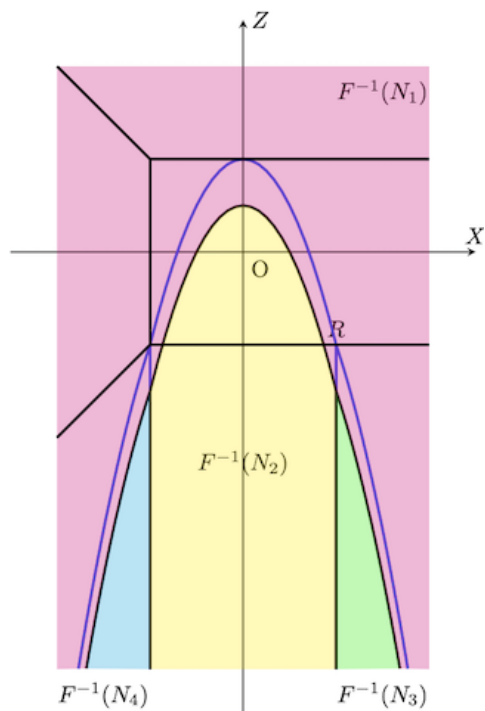


Figure 6: The inverse images of each domain. The same set of parameters is used as in Fig. 5. The blue curve represents the uppermost situation.

thus it is mapped by F^{-1} as

$$F^{-1}(N_4) = \{(X, Y, Z, W) \mid Z = A_0 - (X^2 + Y^2) - X - \gamma, \gamma \geq 0, X \leq -R\}. \quad (4.23)$$

For $\gamma \geq 0$, we find that $Z - X = A_0 - (X^2 + Y^2) - X - \gamma - X \leq A_0 - X^2 - 2X \leq 0$. Here we have again used lemma 4.1 and $X \leq -R$ in the region $F^{-1}(N_4)$. Since the points in $F^{-1}(N_4)$ satisfy $X \leq -R$ and $Z \leq X$, $F^{-1}(N_4) \subset N_4$ holds.

f) It is easy to see that $F^{-1}(N_2)$ is contained in the region $|X| \leq R$. Combining these facts with the definitions of N_1, N_2 and N_3 , one can show that $F^{-1}(N_2) \in N_2 \cup N_3 \cup N_4$ holds (see Fig. 6). \square

4.3. Existence domain of the non-wandering set: proof of Main theorem 3.1 A-1) and Main theorem 3.2 B-1)

In this section, based on Proposition 4.4, we specify the domain containing the non-wandering set $\Omega(F)$. As illustrated in Fig. 7 the flow of dynamics, regardless of whether the flow from N_4 to N_2 exists or not, an orbit launched in the domain N_3 does not return back to the vicinity of the initial point. Propositions 4.4 a) implies that the coordinate X of the points contained in N_1 are strictly decreasing, and also 4.4 d) implies the coordinate Z of the points contained in N_4 are strictly increasing, so they do not return back to the vicinity of the initial points as well. This argument holds for the backward iteration F^{-1} . It follows that the points of the non-wandering set $\Omega(F)$ do not exist in

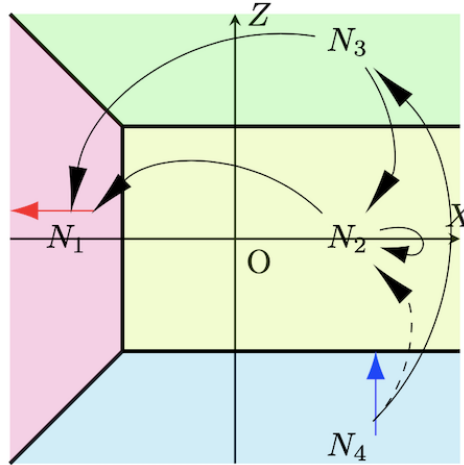


Figure 7: The flow of dynamics. The dashed line shows that the flow can exist, but its proof is not given here. The red and blue arrows indicate a monotonic shift to the left and upward, respectively, in each region.

the domains N_1, N_3 and N_4 , and thus the non-wandering set $\Omega(F)$ should be contained in the domain N_2 .

Since $\Omega(F) \subset N_2$, the non-wandering set can be expressed as $\Omega(F) = \Lambda \subset \bigcap_{k=-\infty}^{\infty} F^k(N_2)$, thus $\Omega(F) \subset F^{-1}(N_2) \cap N_2 \cap F(N_2)$ holds. Note here that we do not know whether the non-wandering set is empty or not. In the following, we use this condition to further specify the existence domain of the non-wandering set. More specifically, we will provide a hypercube containing the region $F^{-1}(N_2) \cap N_2 \cap F(N_2)$.

First, note that the non-wandering set $\Omega(F)$ should be located in the region $|Z| \leq R$, since $\Omega(F) \subset F^{-1}(N_2) \cap N_2 \cap F(N_2)$. From the mapping rule (2.5), $|Z_0| \leq R$ immediately leads to $|X_{-1}| \leq R$. Therefore, the condition $\Omega(F) \subset F^{-1}(N_2)$ implies that $|X| \leq R$ must be satisfied for the points in $\Omega(F)$ (see Fig. 6).

Next, we recall (4.17), which tells us the maximum value of X in the region $F(N_2)$, that is,

$$\begin{aligned} X_1 &= A_0 - (Z_1^2 + W_1^2) + R \\ &\leq A_0 - W_1^2 + R. \end{aligned} \quad (4.24)$$

The condition $|X_1| \leq R$, obtained above, leads to

$$-R \leq A_0 - W_1^2 + R, \quad (4.25)$$

which implies that $|W_1| \leq R$ must be satisfied for the points in $\Omega(F)$ (see Fig. 8(a)). Again, it follows immediately from the mapping rule (2.5) that $|Y_0| \leq R$.

As a result of these arguments, we can conclude that

$$\Omega(F) \subset V_F = \{(X, Y, Z, W) \mid |X|, |Y|, |Z|, |W| \leq R\}. \quad (4.26)$$

We then consider the hypercube V_f in the original coordinates (x, y, z, w) , which contains the region V_F . The slice of V_f by (x, y) -plane is illustrated in Fig. 9, and we have

$$\Omega(f) \subset V_f = \{(x, y, z, w) \mid |x|, |y|, |z|, |w| \leq 2\sqrt{2}R\}. \quad (4.27)$$

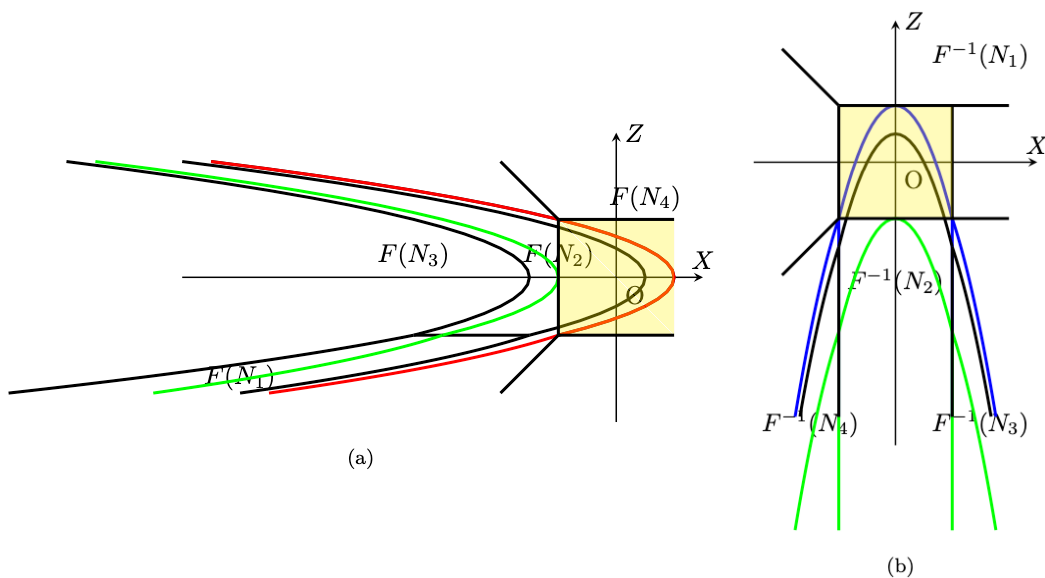


Figure 8: The domains mapped by F and F^{-1} . (a) The green curve shows the leftmost parabola for which $N_2 \cap F(N_2) \neq \emptyset$. (b) The green curve shows the lowest parabola for which $N_2 \cap F^{-1}(N_2) \neq \emptyset$.

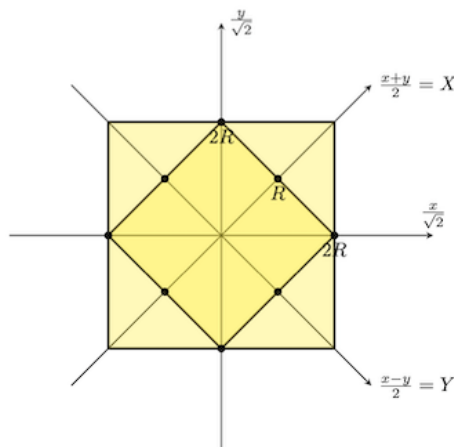


Figure 9: Domains containing the non-wandering set $\Omega(F)$.

The proof of our Main theorems 3.1 A-1) and 3.2 B-1) is thus completed.

5. Sufficient condition for uniform hyperbolicity

5.1. Cone field condition

We introduce here the cone field condition [42], which leads to a sufficient condition for uniform hyperbolicity.

Definition 5.1. Let $\mathbb{E}_1 \subset \mathbb{R}^n$ and \mathbb{E}_2 be a proper subspace and its complementary subspace, respectively. i.e., $\mathbb{R}^n = \mathbb{E}_1 \oplus \mathbb{E}_2$. The standard unit cone determined by the

subspaces \mathbb{E}_1 and \mathbb{E}_2 is given by the set,

$$K(\mathbb{E}_1, \mathbb{E}_2) = \{\mathbf{v} = (\mathbf{v}_1, \mathbf{v}_2) \mid \mathbf{v}_1 \in \mathbb{E}_1, \mathbf{v}_2 \in \mathbb{E}_2, |\mathbf{v}_2| \leq |\mathbf{v}_1|\}. \quad (5.1)$$

Definition 5.2. A cone in \mathbb{R}^n with core \mathbb{E}_1 , denoted by $\mathcal{C}(\mathbb{E}_1)$, is the image $T(K(\mathbb{E}_1, \mathbb{E}_2))$. Here $T : \mathbb{R}^n \rightarrow \mathbb{R}^n$ is a linear automorphism such that $T(\mathbb{E}_1) = \mathbb{E}_1$. By a cone \mathcal{C} in \mathbb{R}^n we mean a set $\mathcal{C}(\mathbb{E}_1)$ for some proper subspace \mathbb{E}_1 of \mathbb{R}^n .

Definition 5.3. A cone field $\mathcal{C} = \{\mathcal{C}_x\}$ on a manifold M is a collection of cones $\mathcal{C}_x \in T_x M$ for $x \in M$.

Definition 5.4. For a given cone field $\mathcal{C} = \{\mathcal{C}_x\}_{x \in M}$ and a diffeomorphism h defined on the manifold M , let

$$m_{\mathcal{C},x} = m_{\mathcal{C},x}(h) = \inf_{\mathbf{v} \in \mathcal{C}_x \setminus \{0\}} \frac{|Dh_x(\mathbf{v})|}{|\mathbf{v}|}, \quad (5.2)$$

$$m'_{\mathcal{C},x} = m'_{\mathcal{C},x}(h) = \inf_{\mathbf{v} \notin \mathcal{C}_{h(x)}} \frac{|Dh_{h(x)}^{-1}(\mathbf{v})|}{|\mathbf{v}|}. \quad (5.3)$$

We call $m_{\mathcal{C},x}$ and $m'_{\mathcal{C},x}$ the minimal expansion and minimal co-expansion of h on \mathcal{C}_x , respectively.

Definition 5.5. We say that h is expanding on the cone field \mathcal{C} if

$$\inf_{x \in \Lambda} m_{\mathcal{C},x}(h) > 1 \iff \inf_{x \in \Lambda} \inf_{\mathbf{v} \in \mathcal{C}_x \setminus \{0\}} \frac{|Dh_x(\mathbf{v})|}{|\mathbf{v}|} > 1. \quad (5.4)$$

Similarly, we say that h is co-expanding on the cone field \mathcal{C} if

$$\inf_{x \in \Lambda} m'_{\mathcal{C},x}(h) > 1 \iff \sup_{x \in \Lambda} \sup_{\mathbf{u} \in Dh_{h(x)}^{-1}(\mathcal{C}_{h(x)})} \frac{|Dh_x(\mathbf{u})|}{|\mathbf{u}|} < 1. \quad (5.5)$$

Definition 5.6. We say that the cone field \mathcal{C}_x has constant orbit core dimension on Λ if

$$\dim \mathbb{E}_x = \dim \mathbb{E}_{h(x)} \quad (5.6)$$

holds for all $x \in \Lambda$. Here \mathbb{E}_x and $\mathbb{E}_{h(x)}$ are the cores of \mathcal{C}_x and $\mathcal{C}_{h(x)}$, respectively.

Based on these notions, Newhouse has derived a necessary and sufficient condition for uniform hyperbolicity.

Theorem 5.7 (Newhouse). *A sufficient condition for $\Lambda(h)$ to be uniformly hyperbolic is that there are an integer $N > 0$ and a cone field \mathcal{C} with constant orbit core dimension over $\Lambda(h)$ such that h^N is both expanding and co-expanding on \mathcal{C} .*

Here we can show the following.

Corollary 5.8. *If there exists a standard unit cone field \mathcal{C}_x on $\Lambda(h)$ with h -invariant cones, i.e., $Dh(\mathbb{E}_x) = \mathbb{E}_{h(x)}$, $\forall x \in \Lambda(h)$, such that h is both expanding and co-expanding, then $\Lambda(h)$ is uniformly hyperbolic.*

Proof. Since \mathbb{E}_x is invariant under h , it has constant orbit core dimension. The fact that for any $x \in \Lambda(h)$ $\lambda \leq m_{\mathcal{C},x}$ and $\lambda \leq m'_{\mathcal{C},x}$ imply that h is both expanding and co-expanding. Hence h is uniformly hyperbolic. \square

5.2. Sufficient condition for uniform hyperbolicity: the case with four symbols in the anti-integrable limit

We first derive a sufficient condition for the case whose anti-integrable limit has four symbols. The Jacobian for the forward and backward iterations is respectively given by

$$Jf = \begin{pmatrix} -2x + c & -c & -1 & 0 \\ -c & -2y + c & 0 & -1 \\ 1 & 0 & 0 & 0 \\ 0 & 1 & 0 & 0 \end{pmatrix}, \quad (5.7)$$

$$Jf^{-1} = \begin{pmatrix} 0 & 0 & 1 & 0 \\ 0 & 0 & 0 & 1 \\ -1 & 0 & -2z + c & -c \\ 0 & -1 & -c & -2w + c \end{pmatrix}. \quad (5.8)$$

The following lemma will be used in the subsequent argument.

Lemma 5.9. *Let*

$$G(x, y) = \begin{pmatrix} -2x + c & -c \\ -c & -2y + c \end{pmatrix}, \quad (5.9)$$

where $x, y \in \mathbb{R}$ satisfy the condition $2\lambda + 2 + c \leq |x|, |y|$. Then, for any vector $\mathbf{w}_0 = (\xi, \eta)^t$, the following holds:

$$(2\lambda + 2)|\mathbf{w}_0| \leq |\mathbf{w}_1|, \quad (5.10)$$

where $\mathbf{w}_1 = G(x, y)\mathbf{w}_0$.

Proof. In the case $|\eta_0| \leq |\xi_0|$, we have

$$\begin{aligned} |\mathbf{w}_1| &\geq |\xi_1| \\ &= |(-2x + c)\xi_0 - c\eta_0| \\ &\geq |-(2x - c)\xi_0| - |c\eta_0| \\ &= |(2x - c)||\xi_0| - c|\eta_0| \\ &\geq (2|x| - c)|\xi_0| - c|\eta_0| \\ &\geq 2(|x| - c)|\xi_0| \\ &= (|x| - c)(|\xi_0| + |\xi_0|) \\ &\geq (|x| - c)(|\xi_0| + |\eta_0|) \\ &\geq (|x| - c)|\mathbf{w}_0| \\ &\geq (2\lambda + 2)|\mathbf{w}_0|. \end{aligned}$$

Similarly, for $|\xi_0| < |\eta_0|$,

$$\begin{aligned} |\mathbf{w}_1| &\geq |\eta_1| \\ &= |-c\xi_0 + (-2y + c)\eta_0| \end{aligned}$$

$$\begin{aligned}
 &\geq |-(2y - c)\eta_0| - |c\xi_0| \\
 &= |(2y - c)\eta_0| - |c\xi_0| \\
 &\geq (2|y| - c)|\eta_0| - |c\xi_0| \\
 &\geq 2(|y| - c)|\eta_0| \\
 &= (|y| - c)(|\eta_0| + |\eta_0|) \\
 &\geq (|y| - c)(|\xi_0| + |\eta_0|) \\
 &\geq (|y| - c)|\mathbf{w}_0| \\
 &\geq (2\lambda + 2)|\mathbf{w}_0|.
 \end{aligned}$$

□

Suppose that $\mathbb{E}^+, \mathbb{E}^- \subset \mathbb{R}^2$ gives $\mathbb{R}^4 = \mathbb{E}^- \oplus \mathbb{E}^+$. For $K = K(\mathbb{E}^+, \mathbb{E}^-)$, we can show the following.

Theorem 5.10. *Suppose that the matrix $G(x, y)$ satisfies the condition,*

$$(2\lambda + 2)|\mathbf{v}| \leq |G(x, y)\mathbf{v}|, \quad (5.11)$$

for some $\lambda > 1$ and any vector $\mathbf{v} \in \mathbb{R}^2$. In addition, Jf and Jf^{-1} are expressed in terms of the 2×2 identity matrix I_2 and the zero matrix O_2 as

$$Jf = \begin{pmatrix} G(x, y) & -I_2 \\ I_2 & O_2 \end{pmatrix}, \quad (5.12)$$

$$Jf^{-1} = \begin{pmatrix} O_2 & I_2 \\ -I_2 & G(z, w) \end{pmatrix}, \quad (5.13)$$

then the following holds:

- a) For any vector $\mathbf{v}_0 \in K$, $\lambda|\mathbf{v}_0| \leq |\mathbf{v}_1|$ holds where $\mathbf{v}_1 = Jf(\mathbf{v}_0)$.
- b) For any vector $\mathbf{v}_0 \notin K$, $\lambda|\mathbf{v}_0| \leq |\mathbf{v}_{-1}|$ holds where $\mathbf{v}_{-1} = Jf^{-1}(\mathbf{v}_0)$.

Proof. For a), we have

$$\begin{aligned}
 |\mathbf{v}_1| &= \left| \begin{pmatrix} G(x, y)\mathbf{v}_0^+ - \mathbf{v}_0^- \\ \mathbf{v}_0^+ \end{pmatrix} \right| \\
 &\geq |G(x, y)\mathbf{v}_0^+ - \mathbf{v}_0^-| - |\mathbf{v}_0^+| \\
 &\geq |G(x, y)\mathbf{v}_0^+| - |\mathbf{v}_0^-| - |\mathbf{v}_0^+| \\
 &\geq (2\lambda + 1)|\mathbf{v}_0^+| - |\mathbf{v}_0^-| \\
 &\geq 2\lambda|\mathbf{v}_0^+| \\
 &\geq \lambda(|\mathbf{v}_0^+| + |\mathbf{v}_0^-|) \\
 &\geq \lambda|\mathbf{v}_0|.
 \end{aligned}$$

Similarly, for b), we have

$$|\mathbf{v}_{-1}| = \left| \begin{pmatrix} \mathbf{v}_0^- \\ -\mathbf{v}_0^+ + G(z, w)\mathbf{v}_0^- \end{pmatrix} \right|$$

$$\begin{aligned}
 &\geq |G(z, w)\mathbf{v}_0^- - \mathbf{v}_0^+| - |\mathbf{v}_0^-| \\
 &\geq |G(z, w)\mathbf{v}_0^-| - |\mathbf{v}_0^+| - |\mathbf{v}_0^-| \\
 &\geq (2\lambda + 1)|\mathbf{v}_0^-| - |\mathbf{v}_0^+| \\
 &\geq 2\lambda|\mathbf{v}_0^-| \\
 &\geq \lambda(|\mathbf{v}_0^+| + |\mathbf{v}_0^-|) \\
 &\geq \lambda|\mathbf{v}_0|.
 \end{aligned}$$

□

Theorem 5.10 tells us that f is expanding and co-expanding. Combined with the Lemma 5.9, we finally find the following:

Corollary 5.11. *If all points in the non-wandering set $\Omega(f)$, if not empty, satisfy the condition*

$$4 + c \leq |x|, |y|, |z|, |w|, \quad (5.14)$$

then $\Omega(f)$ is uniformly hyperbolic.

5.3. Sufficient condition for uniformly hyperbolicity: the case with two symbols in the anti-integrable limit

Next, we consider a sufficient condition for the case where the anti-integrable limit has two symbols. The Jacobian after the transformation (2.3) is respectively given by

$$Jf = \begin{pmatrix} \tilde{G}(x, y) & -I_2 \\ I_2 & O_2 \end{pmatrix}, \quad (5.15)$$

$$Jf^{-1} = \begin{pmatrix} O_2 & I_2 \\ -I_2 & \tilde{G}(z, w) \end{pmatrix}. \quad (5.16)$$

The following will be used in the following argument.

Lemma 5.12. *Let*

$$\tilde{G}(X, Y) = \begin{pmatrix} -2X & -2Y \\ -2Y & -2X + 2c \end{pmatrix}, \quad (5.17)$$

where $X, Y \in \mathbb{R}$ satisfy the condition $2\lambda + 2 + c \leq |X| - |Y|$. Then, for any vector $\mathbf{w}_0 = (\xi, \eta)^t$, the following holds:

$$(2\lambda + 2)|\mathbf{w}_0| \leq |\mathbf{w}_1|, \quad (5.18)$$

where $\mathbf{w}_1 = G(x, y)\mathbf{w}_0$.

Proof. In the case $|\eta_0| \leq |\xi_0|$, we have

$$\begin{aligned}
 |\mathbf{w}_1| &\geq |\xi_1| \\
 &= |(-2X)\xi_0 - 2Y\eta_0| \\
 &\geq |-2X\xi_0| - |2Y\eta_0|
 \end{aligned}$$

$$\begin{aligned}
 &\geq 2(|X| - |Y|)|\xi_0| \\
 &= (|X| - |Y|)(|\xi_0| + |\xi_0|) \\
 &\geq (||X| - |Y|)(|\xi_0| + |\eta_0|) \\
 &\geq (|X| - |Y|)|\mathbf{w}_0| \\
 &\geq (2\lambda + 2)|\mathbf{w}_0|.
 \end{aligned}$$

Similarly, for $|\xi_0| < |\eta_0|$,

$$\begin{aligned}
 |\mathbf{w}_1| &\geq |\eta_1| \\
 &= |-2Y\xi_0 - 2(X - c)\eta_0| \\
 &\geq |-2(X - c)||\eta_0| - |-2Y||\xi_0| \\
 &= 2|(X - c)||\eta_0| - 2|Y||\xi_0| \\
 &\geq 2(|X| - c)|\eta_0| - 2|Y||\xi_0| \\
 &> 2(|X| - |Y| - c)|\eta_0| \\
 &= (|X| - |Y| - c)(|\eta_0| + |\eta_0|) \\
 &> (|X| - |Y| - c)(|\xi_0| + |\eta_0|) \\
 &\geq (|X| - |Y| - c)|\mathbf{w}_0| \\
 &\geq (2\lambda + 2)|\mathbf{w}_0|.
 \end{aligned}$$

□

Combining Theorem 5.10 with lemma 5.12, we find the following:

Corollary 5.13. *If all points in the non-wandering set $\Omega(f)$, if not empty, satisfy the condition*

$$4 + c \leq |X| - |Y|, |Z| - |W|, \quad (5.19)$$

then $\Omega(F)$ and so $\Omega(f)$ is uniformly hyperbolic.

6. Proof of Main theorems

6.1. The case with four symbols in the anti-integrable limit

Topological horseshoe:

In this section, we provide a sufficient condition for topological horseshoe and uniform hyperbolicity for the case (A), *i.e.*, the case around the anti-integrable limit with four symbols. First, we consider the situation in the original coordinate (x, y, z, w) . Using the relation $f^{-1}(f(V_f)) = V_f$, we find that the region $f(V_f)$ is expressed as

$$\begin{cases} |z| \leq r, \\ |w| \leq r, \\ |a_0 - z^2 - x + c(z - w)| \leq r, \\ |a_1 - w^2 - y - c(z - w)| \leq r. \end{cases} \quad (6.1)$$

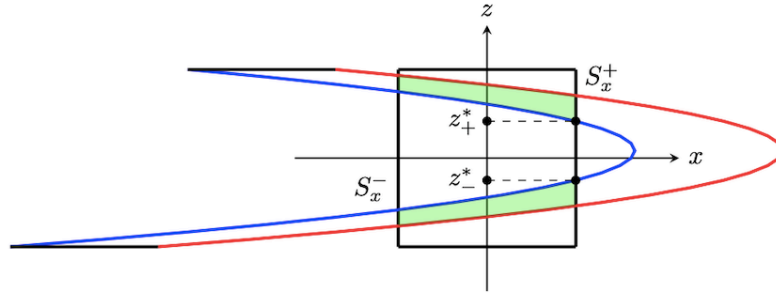


Figure 10: Γ_x in the (x, z) -plane. The red and blue curves represent Γ_x^{\max} and Γ_x^{\min} , respectively. The green regions show $f(V_f) \cap V_f$.

We can re-express $f(V_f)$ as

$$f(V_f) = \{(x, y, z, w) \mid |z| \leq r, |w| \leq r, x = -z^2 + cz + a_0 + \alpha\} \\ \text{where } |\alpha| \leq (c+1)r, y = -w^2 + cw + a_1 + \beta \text{ where } |\beta| \leq (c+1)r\}. \quad (6.2)$$

In this new expression, we have got rid of w -dependence of x or z , as well as the z -dependence of y or w . Therefore the (x, z) -plane is now decoupled from the (y, w) -plane. It is therefore valid to consider parabolas in the (x, z) -plane and the (y, w) -plane, separately.

Let Γ_x^{\max} be the parabola with the largest x (rightmost in Fig. 10), Γ_x^{\min} be the one with the smallest x (leftmost in Fig. 10):

$$\Gamma_x^{\max} : x = -z^2 + cz + a_0 + (c+1)r, \quad (6.3)$$

$$\Gamma_x^{\min} : x = -z^2 + cz + a_0 - (c+1)r. \quad (6.4)$$

Furthermore, let $S_x^+ = \{(x, y, z, w) \in V \mid x = r\}$ and $S_x^- = \{(x, y, z, w) \in V \mid x = -r\}$, respectively (see Fig. 10). For the 2-dimensional Hénon map f , the horseshoe condition is given by the requirement that $f \cap f(V)$ is decomposed into two disjoint regions. Here the region V is a region that contains the non-wandering set $\Omega(f)$. Here we apply the same condition for the (x, z) - and (y, w) -planes, respectively. First we consider the condition for the (x, z) -plane. In order for the horseshoe condition to be satisfied in the (x, z) -plane, as shown in Fig. 10, the following should hold:

- 1) Γ_x^{\min} intersects S_x^+ at two points.
- 2) Γ_x^{\max} intersects S_x^- at two points.

The first condition holds if

$$\frac{1}{4}c^2 + a_0 - (c+1)r > r \quad (6.5)$$

is satisfied. Since it is assumed that $c > 0$, the second condition is equivalent to the condition requiring that $x(z = r) \leq -r$ and $x(z = -r) \leq -r$. The former condition is written as

$$-r^2 + cr + a_0 + (c+1)r \leq -r. \quad (6.6)$$

The latter condition automatically holds if the former one is fulfilled.

The argument for the (y, w) -plane is developed in the same way, again based on (6.1), which leads to the conditions

$$\frac{1}{4}c^2 + a_1 - (c + 1)r > r, \quad (6.7)$$

$$-r^2 + cr + a_1 + (c + 1)r \leq -r. \quad (6.8)$$

Due to the symmetry, the inverse map f^{-1} is obtained by swapping $(x, y) \leftrightarrow (z, w)$ in the map f , thus the same conditions follow for f^{-1} . Thus, the conditions (6.5), (6.6), (6.7), and (6.8) lead to a topological horseshoe. The proof of Theorem 3.1 A-1) is done.

Uniform hyperbolicity:

Next, we consider a sufficient condition for uniform hyperbolicity. From section 5.2, to obtain uniform hyperbolicity it is sufficient to show that any point $(x, y, z, w) \in f(V_f) \cap V_f$ satisfies the condition (5.14) since $\Omega(f) \subset f(V_f) \cap V_f$ holds.

Suppose that $(x, y, z, w) \in f(V_f) \cap V_f$, and the conditions (6.5) and (6.6) are satisfied. Let z_-^* and z_+^* be the z coordinates of the intersection points between Γ_{\min} and S_x^+ where $z_-^* \leq z_+^*$ is assumed (see Fig. 10). We can explicitly obtain as

$$z_{\pm}^* = \frac{c \pm \sqrt{c^2 + 4(a_0 - (c + 2)r)}}{2}. \quad (6.9)$$

If $z_-^* < 0$, the following holds:

$$|z| \geq \min(|z_-^*|, |z_+^*|) = |z_-^*| = -z_-^*.$$

Here $c > 0$ is used to show the first inequality. Hence, if the condition

$$-z_-^* > 4 + c \quad (6.10)$$

is satisfied, then $|z| > 4 + c$ holds for all the points in $f(V) \cap V$. Note that the condition (6.10) automatically ensures the condition $z_-^* < 0$ for $c > 0$.

We can develop the same argument for the (y, w) -plane, and find that the following is sufficient to ensure that the condition $|w| > 4 + c$ holds for all the points within $f(V) \cap V$:

$$\frac{-c + \sqrt{c^2 + 4(a_1 - (c + 2)r)}}{2} > 4 + c. \quad (6.11)$$

In a similar manner, the argument for the inverse map f^{-1} provides a sufficient condition to satisfy $|x|, |y| > 4 + c$. Since the inverse map f^{-1} is given by swapping the variables as $(x, y) \leftrightarrow (z, w)$, the resulting conditions are the same as (6.10) and (6.11). Thus, in addition to the conditions (6.5), (6.6), (6.7), and (6.8) the conditions (6.10) and (6.11) lead to a sufficient condition for the non-wandering set $\Omega(f)$ to be uniformly hyperbolic. The proof of Theorem 3.1 A-2) is complete.

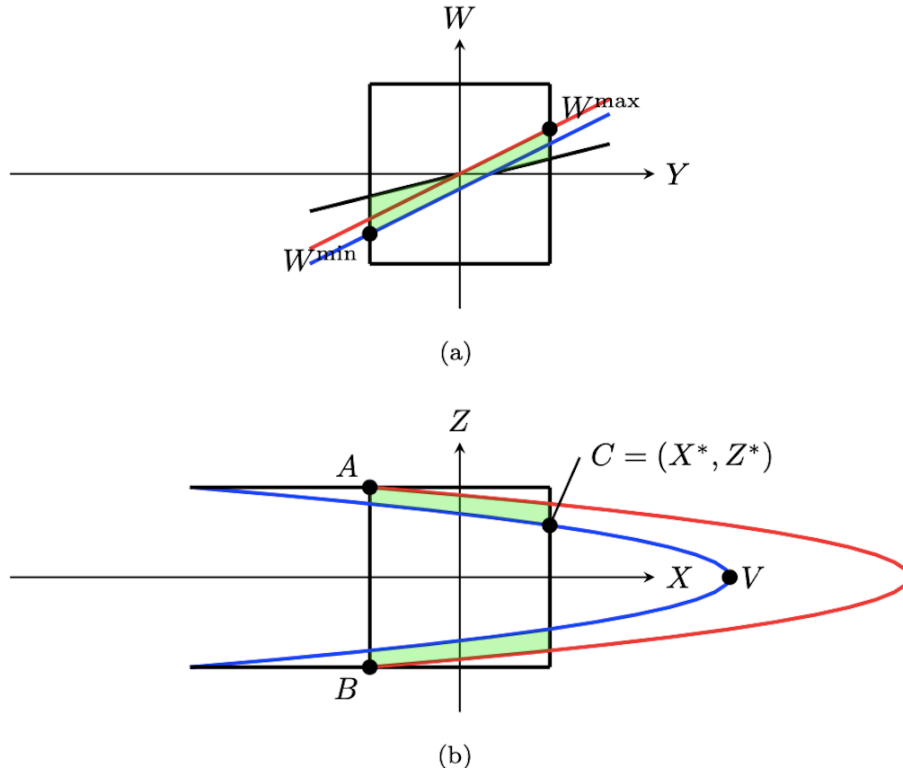


Figure 11: (a) Projection of $F(V_F) \cap V_F$ onto the (Y, W) -plane (green). The red and blue curves illustrate Γ_Y^{\max} and Γ_Y^{\min} , respectively. (b) Projection of $F(V_F) \cap V_F$ onto the (X, Z) -plane. The red and blue curves illustrate Γ_X^{\max} and Γ_X^{\min} , respectively.

6.2. The case with two symbols in the anti-integrable limit

Topological horseshoe:

We first examine the existence of topological horseshoe. From the definition (3.16) of V_F and the mapping rule (2.4), we have

$$\begin{aligned} F(V_F) \cap V_F = \{ & (X, Y, Z, W) \mid |X|, |Y|, |Z|, |W| \leq R, \\ & X = -Z^2 - W^2 + A_0 + s', |s'| \leq R, \\ & Y = A_1 + 2(c - Z)W + s, |s| \leq R\}. \end{aligned} \quad (6.12)$$

First, consider the projection of $F(V_F) \cap V_F$ onto the (Y, W) -plane. Let

$$\Gamma_Y : Y = A_1 - 2(c - Z)W + s, \quad (6.13)$$

be a set of straight lines in the (Y, W) -plane parametrized by Z and s , where $|s| \leq R$, and let

$$\Gamma_Y^{\max} : Y = A_1 + 2(c - R)W - R, \quad (6.14)$$

$$\Gamma_Y^{\min} : Y = A_1 + 2(c - R)W + R, \quad (6.15)$$

be the upper and lower straight members of Γ_Y . Γ_Y^{\max} is attained at $Z = R$ and $s = -R$, and Γ_Y^{\min} is attained at $Z = R$ and $s = R$ (see Fig 11(a)). Since $c > R$ and $|Z| \leq R$, we

know that the slope of Γ_Y is always positive. Solving for W , we get

$$W = \frac{Y - A_1 - s}{2(c - Z)}. \quad (6.16)$$

The maximum and minimum values of W , denoted by W_{\max} and W_{\min} respectively, are given as

$$W_{\max} = \frac{2R - A_1}{2(c - R)}, \quad \text{attained at } Y = R, Z = R \text{ and } s = -R, \quad (6.17)$$

$$W_{\min} = \frac{-2R - A_1}{2(c - R)}, \quad \text{attained at } Y = -R, Z = R \text{ and } s = R. \quad (6.18)$$

Since we have imposed the condition (3.19), we see that the projection of $F(V_F)$ intersects V_F completely in the Y -direction, and the width of $F(V_F) \cap V_F$, as measured in the W -direction, is strictly less than $2R$ (see Fig 11(a)).

Next, consider the projection of $F(V_F) \cap V_F$ onto the (X, Z) -plane. Let

$$\Gamma_X : X = -Z^2 - W^2 + A_0 + s' \quad (6.19)$$

be a family of parabolas in the (X, Z) -plane parametrized by W and s' , where $|W| \leq W^*$ and $|s'| \leq R$. Let

$$\Gamma_X^{\max} : X = -Z^2 + A_0 + R, \quad (6.20)$$

$$\Gamma_X^{\min} : X = -Z^2 + A_0 - (W^*)^2 - R, \quad (6.21)$$

be the rightmost and leftmost members of Γ_X . Note that Γ_X^{\max} is attained at $W = 0$ and $s' = R$, and Γ_X^{\min} at $W = W^*$ and $s' = -R$ (see Fig. 11(b)). For Γ_X^{\max} , notice that when $Z = \pm R$, we have

$$X = -R^2 + A_0 + R = -R. \quad (6.22)$$

Therefore, Γ_X^{\max} intersects with boundary of V_F at its two corner points, namely, $A = (-R, R)$ and $B = (-R, -R)$ in Fig. 11(b).

In the meantime, for Γ_X^{\min} , we examine the location of its vertex, denoted by V in Fig. 11(b). The vertex is attained by setting $Z = 0$, which leads to

$$X_V = A_0 - (W^*)^2 - R.$$

Since it is imposed in (3.18) that

$$A_0 - (W^*)^2 - R > R,$$

we obtain $X_V > R$, i.e., the vertex of Γ_X^{\min} is located on the right side of $(R, 0)$, as illustrated in Fig. 11(b).

As a result, the region in between Γ_X^{\max} and Γ_X^{\min} gives rise to a topological binary horseshoe in the (X, Z) -plane. Thus, we know that the non-wandering set $\Omega(F)$ is non-empty and is at least semi-conjugate to a full shift with two symbols.

Uniform hyperbolicity:

Next, we will show uniform hyperbolicity on $\Omega(F)$. From section 5.3, we already know

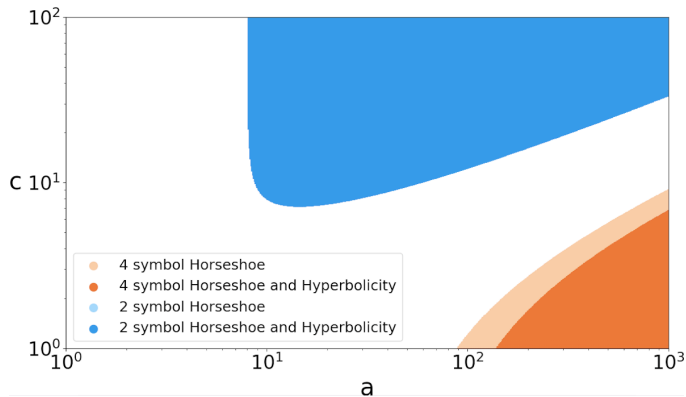


Figure 12: For the anti-integrable limit with four symbols, the region satisfying the topological horseshoe is shown in light orange, and the region satisfying both topological horseshoe and uniform hyperbolicity is shown in orange. For the the anti-integrable limit with two symbols, the region satisfying topological horseshoe is shown in light blue, and the region satisfying both topological horseshoe and uniform hyperbolicity is shown in blue. $a = a_0 = a_1$ are taken.

a sufficient condition for uniform hyperbolicity in Corollary 5.13. Here we show that this is indeed the case for points in $F(V_F) \cap V_F$.

Notice that for any point in $F(V_F) \cap V_F$, we have

$$|Z| \geq Z^*, \quad (6.23)$$

where Z^* is the Z -coordinate of the point C in Fig 11(b). Thus,

$$|Z| - |W| \geq Z^* - |W| \geq Z^* - W^* \quad (6.24)$$

holds. Since it is imposed in (3.20) that $Z^* - W^* \geq 4 + c$, we immediately obtain

$$|Z| - |W| \geq 4 + c. \quad (6.25)$$

Due to the symmetry of the mapping equations, F^{-1} can be obtained from F by swapping (X, Z) with (Y, W) , thus we obtain,

$$|X| - |Y| \geq 4 + c \quad (6.26)$$

as well. The uniform hyperbolicity on $\Omega(F)$ thus follows.

Finally, we check that the parameters leading to the anti-integrable limit satisfy the sufficient condition obtained above for topological horseshoe and uniform hyperbolicity. The case (A) is given by taking the limit of $a = a_0 = a_1 \rightarrow \infty$. This limit implies that $r \rightarrow 2\sqrt{2a}$, so it turns out that the conditions in A-2) and A-3) in Theorem 3.1 hold. For the case (B), the anti-integrable limit is obtained by taking the limit of $a = a_0 = a_1 \rightarrow \infty$ and $\gamma \rightarrow \infty$ with $c = \gamma\sqrt{a}$ being fixed. In this case, $R \rightarrow \sqrt{a}$, $W^* \rightarrow 0$ and $Z^* = \sqrt{a}$ follow, and the conditions in B-2) and B-3) in Theorem 3.2 are

satisfied. Figure 12 illustrates the parameter regions in which topological horseshoe and uniform hyperbolicity hold.

7. Summary

We have derived a sufficient condition for topological horseshoe and uniform hyperbolicity of the coupled Hénon map around the anti-integrable limits. The coupled Hénon map introduced here has at least two types of anti-integrable limits, which were obtained by taking appropriate limits on the nonlinear parameters a_0 , a_1 and a coupling strength c . The strategy of specifying the existence domain of the non-wandering set, and showing topological horseshoe and uniform hyperbolicity is a straightforward generalization of the approach taken in Ref. [6]. It is specific to higher dimensional maps to have different types of horseshoe, and it does not happen in 2-dimensional maps. In a subsequent paper [33], we will further introduce topologically different types of horseshoe that are impossible in two dimensions by studying a family of Hénon-type mappings.

Since the conditions obtained are sufficient ones, as in the case of the 2-dimensional Hénon map [6], one can expect that the parameter domain with topological horseshoe and uniform hyperbolicity must be further extended, possibly to the situation where an analog of the first tangency happens [7, 43]. A plausible approach to this problem would be to use a computer-assisted proof developed in Refs. [8, 9]. Furthermore, it is interesting to investigate the transition between the two types of horseshoes found in the present work. Such a transition, if it exists, will induce a kind of bifurcation in higher dimensions.

Another question to be addressed in the future is whether other types of horseshoes exist in the parameter space. We have studied here only in the symmetric situation $a_0 = a_1$, but it is by no means obvious whether the situation associated with three symbols appears or not. If this is the case, this also provides a new type of horseshoe, which appears only in higher dimensional maps.

Acknowledgement

J.L. and A.S. acknowledge financial support from Japan Society for the Promotion of Science (JSPS) through JSPS Postdoctoral Fellowship for Research in Japan (Standard). This work has been supported by JSPS KAKENHI Grant No. 17K05583, and also by JST, the establishment of university fellowships towards the creation of science technology innovation, Grant Number JPMJFS2139.

References

- [1] Hénon M 1969 Numerical study of quadratic area-preserving mappings *Quarterly of applied mathematics* 291–312

- [2] Hénon M 1976 A two-dimensional mapping with a strange attractor *Communications in Mathematical Physics* **50** 69-77
- [3] Katok A and Hasselblatt B 1995 *Introduction to the modern theory of dynamical systems* (Cambridge: Cambridge University Press)
- [4] Wiggins S 1988 *Global bifurcations and chaos: analytical methods* (Springer-Verlag)
- [5] Wiggins S 2003 *Introduction to applied nonlinear dynamical systems and chaos* (Springer)
- [6] Devaney R and Nitecki Z 1979 Shift automorphisms in the Hénon mapping *Communications in Mathematical Physics* **67** 137-146
- [7] Bedford E and Smillie J 2004 Real polynomial diffeomorphisms with maximal entropy: Tangencies *Annals of mathematics* **160** 1-26
- [8] Arai Z 2007 On hyperbolic plateaus of the Hénon map *Experimental Mathematics* **16** 181-188
- [9] Arai Z 2007 On Loops in the Hyperbolic Locus of the Complex Hénon Map and Their Monodromies *arXiv preprint arXiv:0704.2978*
- [10] Aubry S and Abramovici G 1990 Chaotic trajectories in the standard map. The concept of anti-integrability *Physica D: Nonlinear Phenomena* **43** 199-219
- [11] Aubry S 1994 The concept of anti-integrability applied to dynamical systems and to structural and electronic models in condensed matter physics *Physica D: Nonlinear Phenomena* **71** 196-221
- [12] Bolotin S V and Treschev D V 2015 The anti-integrable limit *Russian Mathematical Surveys* **70** 975-1030
- [13] Aubry S, MacKay R S and Baesens C equivalence of uniform hyperbolicity for symplectic twist maps and phonon gap for Frenkel-Kontorova models *Physica D: Nonlinear Phenomena* **56** 123-134
30
- [14] Mao J 1988 Standard form of four-dimensional symplectic quadratic maps *Physical Review A* **38** 525-526
- [15] Howard J E and MacKay R S 1987 Linear stability of symplectic maps *Journal of mathematical physics* **5** 1036-1051
- [16] Ding M, Bountis T and Ott E 1990 Algebraic escape in higher dimensional Hamiltonian system *Physics Letters A* **151** 395-400
- [17] Bountis T and Kollmann M 1994 Diffusion rates in a 4-dimensional mapping model of accelerator dynamics *Physica D: Nonlinear Phenomena* **71** 122-131
- [18] Todesco E 1994 Analysis of resonant structures of four-dimensional symplectic mappings, using normal forms *Physical Review E* **50** R4298-R4302
- [19] Vrahatis M N, Bountis T C and Kollmann M 1996 Periodic orbits and invariant surfaces of 4D nonlinear mappings *International Journal of Bifurcation and Chaos* **6** 1425-1437
- [20] Todesco E 1996 Local analysis of formal stability and existence of fixed points in 4d symplectic mappings *Physica D: Nonlinear Phenomena* **95** 1-12
- [21] Gemmi M and Todesco E 1997 Stability and geometry of third-order resonances in four-dimensional symplectic mappings *Celestial Mechanics and Dynamical Astronomy* **67** 181-204
- [22] Vrahatis M N, Isliker H and Bountis, T C 1997 Structure and breakdown of invariant tori in a 4-D mapping model of accelerator dynamics *International Journal of Bifurcation and Chaos* **7** 2707-2722
- [23] Giovannozzi M, Scandale W and Todesco E 1998 Dynamic aperture extrapolation in the presence of tune modulation *Physical Review E* **57** 3432-3443
- [24] Richter M, Lange S, Bäcker A and Ketzmerick R 2014 Visualization and comparison of classical structures and quantum states of four-dimensional maps *Physical Review E* **89** 022902
- [25] Lange S, Richter M, Onken F, Bäcker A and Ketzmerick R 2014 Global structure of regular tori in a generic 4D symplectic map *Chaos: An Interdisciplinary Journal of Nonlinear Science* **24** 024409
- [26] Onken F, Lange S, Ketzmerick R and Bäcker, A 2016 Bifurcations of families of 1D-tori in 4D symplectic maps *Chaos: An Interdisciplinary Journal of Nonlinear Science* **26** 063124
- [27] Lange S, Bäcker A and Ketzmerick, R What is the mechanism of power-law distributed Poincaré

- recurrences in higher-dimensional systems? *EPL (Europhysics Letters)* **116** 30002
- [28] Anastassiou S, Bountis T and Bäcker, A 2017 Homoclinic points of 2D and 4D maps via the parametrization method *Nonlinearity* **30** 3799
- [29] Bäcker A and Meiss J E 2018 Moser’s quadratic, symplectic map *Regular and Chaotic Dynamics* **23** 654–664
- [30] Bäcker A and Meiss J E 2020 Elliptic Bubbles in Moser’s 4D Quadratic Map: The Quadfurcation *SIAM Journal on Applied Dynamical Systems* **19** 442–479
- [31] Friedland S and Milnor J 1989 Dynamical properties of plane polynomial automorphisms *Ergodic Theory and Dynamical Systems* **8** 67–99
- [32] Moser J 1994 On quadratic symplectic mappings *Mathematische Zeitschrift* **216** 417–4
- [33] Li J, Fujioka K, and Shudo A 2023 Coupled Hénon Map, Part II: Doubly and Singly Folded Horseshoes in Four Dimensions, *to be submitted*
- [34] Qin W X 2001 Chaotic invariant sets of high-dimensional Hénon-like maps *Journal of mathematical analysis and applications* **264** 76–84
- [35] Aubry S 1995 Anti-integrability in the dynamical and variational problems *Physica D* **86** 284–296
- [36] Du B, Li, M C and Malkin M I 2006 Topological horseshoes for Arneodo Coulet Tresser maps *Regular and Chaotic Dynamics* **11** 181–190
- [37] Li M C and Malkin M 2006 Topological horseshoes for perturbations of singular difference equations *Nonlinearity* **19** 795–811
- [38] Juang J, Li, M C and Malkin M 2008 Chaotic difference equations in two variables and their multidimensional perturbations *Nonlinearity* **21** 1019–1040
- [39] Chen H J and Li M C 2015 Stability of symbolic embeddings for difference equations and their multidimensional perturbations *Journal of Differential Equations* **258** 906–918
- [40] Chen T H, Lin, W W and Peng C C 2016 Chaotic orbits for differentiable maps near anti-integrable limits *Journal of Mathematical Analysis and Applications* **535** 889–916
- [41] Hampton A E and Meiss J D 2022 Anti-integrability for Three-Dimensional Quadratic Maps *SIAM Journal on Applied Dynamical Systems* **21** 650–675
- [42] Newhouse R 2004 Cone-fields, domination and hyperbolicity *Modern Dynamical Systems and Applications* (Cambridge University Press) 419–432
- [43] Sterling D, Dullin H R and Meiss J D 1999 Homoclinic bifurcations for the Hénon map *Physica D: Nonlinear Phenomena* **134** 153–184